Chin. J. Astron. Astrophys. Vol. 7 (2007), No. 5, 721–732
(*http://www.chjaa.org*)

Chinese Journal of
Astronomy and
Astrophysics

Small-Scale Brightenings in the UV Continuum of an M9.1 Solar Flare *

Lin Wang, Cheng Fang and Ming-De Ding

Department of Astronomy, Nanjing University, Nanjing 210093; *wangl@nju.edu.cn*

Received 2007 January 25; accepted 2007 June 19

Abstract We analyze an M9.1 two-ribbon solar flare which occurred on 2004 July 22 using the TRACE white-light and 1700 Å images, the RHESSI, and the SOHO/MDI data. We find many small-scale fast-varying brightenings that appeared in the white-light and 1700 Å images along the flare ribbons. Some of them underwent rapid motions in weak magnetic field regions. We identify these short-lived brightenings as UV continuum enhancement. Our preliminary result shows that the brightenings are closely related to the HXR emission. They have a lifetime of 30–60 s and a typical size of about $1''$–$2''$. The intensity enhancement is about 150–200 times the mean value of the quiet-Sun. According to previous works, we infer that the 1700 Å enhancement may be dominated by the increased emission of 1680 Å continuum coming from the temperature minimum region. The impulsive feature in the 1700 Å light curves of the small-scale brightenings may be due to the irradiation of the impulsive CIV line intensity caused by the bombardment of non-thermal electron beams.

Key words: Sun: activity — Sun: flares — Sun: UV radiation

1 INTRODUCTION

Solar flares are thought to consist of a mass of sub-bursts occurring in the fine magnetic field structures of solar active regions. Investigations on them are important for understanding the nature of solar flares.

The primary process of solar flares is thought to be the so-called elementary flare bursts (EFBs), that reflect small-scale reconnection events occurring catastrophically in the coronal magnetic field. Early observational researches on EFBs paid more attention to the fast spikes in the hard X-ray (HXR) or microwave emissions. Kiplinger et al. (1983) found hundreds of spikes with sub-second duration from a sample of about 3000 HXR solar flares observed by the HXR burst spectrometer on board the *Solar Maximum Mission* (SMM). The duration of the fastest spikes can be as short as 45 ms. Aschwanden et al. (1998) analyzed in detail the HXR and radio elementary temporal structures and their frequency distributions in solar flares. The sub-second temporal structures were even used as a diagnostic tool to study the spatial structures of solar flares (e.g. Aschwanden et al. 1996). Rapid fluctuations are also frequently observed in microwave or decimetric continuum emissions (e.g. Kliem, Karlický & Benz 2000; Nakajima 2000; Fu et al. 2004). However, the observations mentioned above lack spatial resolution and direct information about the corresponding magnetic structures.

The HXR and microwave emissions are known to be emitted by non-thermal electrons that precipitate to the chromosphere through bremsstrahlung or gyrosynchrotron radiation. The chromosphere that is heated and ionized by the electrons can produce Hα emission nearly simultaneously with the HXR bursts (e.g. Canfield & Gayley 1987; Abbett & Hawley 1999). Hence, spatially resolved Hα observations can be used to trace the precipitation sites of the non-thermal electrons that also produce the HXR emission (e.g. Canfield

* Supported by the National Natural Science Foundation of China.

& Gayley 1987; Zhao, Fang & Ding 1997). Trottet et al. (2000) presented a multi-wavelength analysis of an X1.3/2B flare and found that the fast component of Hα emission exhibits time variations with a typical rise time of 0.4–1.5 s which are nearly coincident with the fast HXR pulses. This is convincing evidence for correlated fast temporal structures in the Hα and HXR emissions. Wang et al. (2000) analyzed high-cadence observations of a C5.7 flare and found that the observed high-frequency fluctuations in Hα may be the signature of fine temporal structures related to HXR elementary bursts. Ding et al. (2001) investigated theoretically the origin of the fast component of the fluctuations by a numerical solution of radiative hydrodynamics. These investigations focused more on high temporal resolution rather than high spatial resolution.

Along with the research on fine temporal structures, investigations on fine spatial structures of the footpoints of coronal loops have made some progress. Cheng et al. (1981) first reported HXR-related flare kernels in individual pixels with a size of $4'' \times 4''$ observed in the transition zone lines. A similar phenomenon was found in UV continuum by, e.g., Cheng et al. (1984). Fine structures of footpoints were also reported in Hα observations at early times (e.g., Kanno et al. 1983; Kurokawa et al. 1988).

The *Transition Region and Coronal Explorer* (TRACE) offers an unprecedented opportunity to observe the solar corona and the chromosphere-corona transition region (Handy et al. 1999). Its particular features such as high spatial and high temporal resolutions and a large field of view are conducive to studies on the footpoints of coronal loops. Warren & Warshall (2001) found that the initial HXR burst is positively correlated with UV footpoints that show little or even no preflare activities. Fletcher & Warren (2003) reviewed the features of the UV flare kernels in the impulsive phase, such as the size, the intensity, the motions, and the spatial distributions. Furthermore, Fletcher et al. (2004) discussed the patterns of motion of the footpoints and argued that the excursion from a straight-line trajectory of the motion is partially due to the photospheric structuring of the magnetic field. The authors showed also that the peak times in the brightness is significantly correlated with the peak times in the coronal reconnection rate. These UV brightenings are recently studied by some authors (e.g., Alexander & Coyner 2006).

It seems that most flare observations by TRACE were made in 171 Å, 195 Å, or 1600 Å band before 2003 (Fletcher & Warren 2003). Recently, white-light (WL) and 1700 Å images were used to investigate the white-light flares (e.g., Metcalf et al. 2003; Hudson et al. 2006). In this paper, we analyze the TRACE WL and 1700 Å data of an M9.1 two-ribbon flare on 2004 July 22, which was claimed to be a white-light flare by Hudson et al. (2006). We focus our work on the UV enhancement in the 1700 Å band. We find many small-scale brightenings that appear in the flare ribbons. The 1700 Å light curves of the brightenings show an impulsive feature. The properties of the impulsive feature are determined quantitatively.

We describe the observations and the data reduction in Section 2, present our results in Section 3 and a discussion in Section 4. A brief summary is given in Section 5.

2 OBSERVATIONS AND DATA REDUCTION

An M9.1 two-ribbon flare occurred on 2004 July 22 in the active region NOAA 10652 (N05 °E16°). According to the *Solar Geophysical data* (SGD), the GOES soft X-ray (SXR) flare started at 00:14 UT and ended at 00:43 UT with a peak at 00:32 UT. The observations of the *Large Angle and Spectrometric Coronagraph* (LASCO) on board the *Solar and Heliospheric Observatory* (SOHO) showed that a CME event appeared about one hour after the peak of the flare.

TRACE provides high spatial resolution observations in EUV, UV and broadband white-light continuum (Handy et al. 1999). Observations of the flare were made in 1700 Å and WL channels. The time cadence is about 5 s in each channel during most of the flaring time and the pixel size of the images is $0.5'' \times 0.5''$. The data reduction includes CCD dark current subtraction, flat field correction, normalization of exposure time to 1 s and wavelength-dependent pointing correction. There are some observations in these two channels before the flare and one of the WL images is used for co-alignment purpose (see below).

It should be pointed out that the 1700 Å images tend to be saturated, especially in the flaring regions during the impulsive phase of the flares. Thus, it is necessary to check whether the level 0 images are saturated or not in the quantitative analysis of the 1700 Å data. Actually, saturation was similarly found in other TRACE images (Fletcher & Warren 2003).

In our study, 500 frames of 1700 Å images are checked to be from 2004 July 21 23:30:50 UT to July 22 01:00:32 UT, fully covering the flare period. There are only 63 pixels with values higher than 3000 data number (DN). Thus, we conclude that these data can be safely used in our quantitative analysis.

The *Reuven Ramaty High-Energy Solar Spectroscopic Imager* (RHESSI) provides unprecedented high resolution observations not only in time and space, but also in spectra of SXR, HXR, and γ-rays (Lin et al. 2002). It observed this flare continuously with the attenuators changing several times.

The continuum intensity and line-of-sight magnetic field data observed by the *Michelson Doppler Imager* (MDI) (Scherrer et al. 1995) on board SOHO are used in our work. The continuum image closest in time to this flare was observed at July 21 23:59:32 UT, about half an hour before the flare peak. It is used for the image co-alignment mentioned below. The magnetogram was taken from the 96 minute cadence synoptic observations. It was obtained at 23:59:02 UT, almost simultaneously with the continuum intensity. The pixel size of these data is about $2'' \times 2''$.

To co-align the SOHO/MDI and TRACE data, Metcalf et al. (2003) stated that a cross correlation between the MDI continuum and the TRACE WL images can provide a good result with an alignment accuracy of about $0.5''$. We applied their algorithm to the SOHO/MDI continuum and the TRACE WL image closest in time. The offsets and the roll angle of the WL image to the MDI continuum obtained from the correlation are assumed to be invariable during the observations. Hence the other WL images were shifted and rolled with the same parameters. They were then corrected for the effect of the solar rotation to the time of the MDI image.

3 RESULTS

3.1 General View of the Flare

Figure 1 plots the TRACE WL images at some selected times covering the impulsive phase. They show the evolution of the flare morphology. The green contours in each panel show the UV enhancement observed in the TRACE 1700 Å images closest in time to the WL images. It can be seen that there was obvious UV enhancement in the impulsive phase of the flare. The enhancement exhibits two ribbon-like structures. The whole area of the structures expanded and reached a maximum at 00:30:16 UT, which is around the HXR peak times. Then, the two ribbons rapidly decayed.

Along with the evolution in the 1700 Å images, many strongly enhanced small-scale patches, marked in red color in Figure 1, are found in the WL images from 00:23:41 UT. These patches appear first in a negative magnetic region and then, after 00:26:55 UT, in a positive magnetic region. It seems that almost all the patches are within the two UV ribbons and their size varies in accordance with that of the UV enhancement.

In order to determine the quiescent value of the WL images and rule out possible noise effect, we select a small quiet-Sun region near the flare (shown as a blue square in each panel of Figure 1), to calculate the mean count rate and the standard deviation for the WL images. The square is selected in a region with a weak magnetic field to avoid the effect of faculae, which are always found around sunspots. Considering that there may be small fluctuations caused by the granulation and p-mode oscillations that vary with time, we take all of the pixels in this region as our statistical samples from about 500 WL images, which were taken over a time span of one hour and a half from 2004 July 21 23:30:46 UT to 2004 July 22 01:01:11 UT, that fully cover the flare period. The statistics give a good Gaussian probability density distribution of count rates. Hence, the mean count rate is taken as the quiescent value of WL images. Similarly, we determine the quiescent value of the 1700 Å images.

In this work, WL count rates three standard deviations over the quiescent value are regarded as true signals. The pixels satisfying this criterion are those marked in red in Figure 1. Thus, we are sure that the strong enhancement reflects a certain physical process related to the flare.

3.2 Investigation of a Specified Small Region

We select a small region of $30'' \times 30''$ in the negative magnetic field (marked by the black box in Figure 1). In this small region, small-scale patches appeared frequently around the small sunspots. This region contains many footpoints of flare loops.

When we zoom in, the jitter effect of the TRACE instrument becomes severe. To correct this effect on the WL images, we apply a correlation algorithm given by the TRACE routine, TR_GET_DISP_2D.PRO,

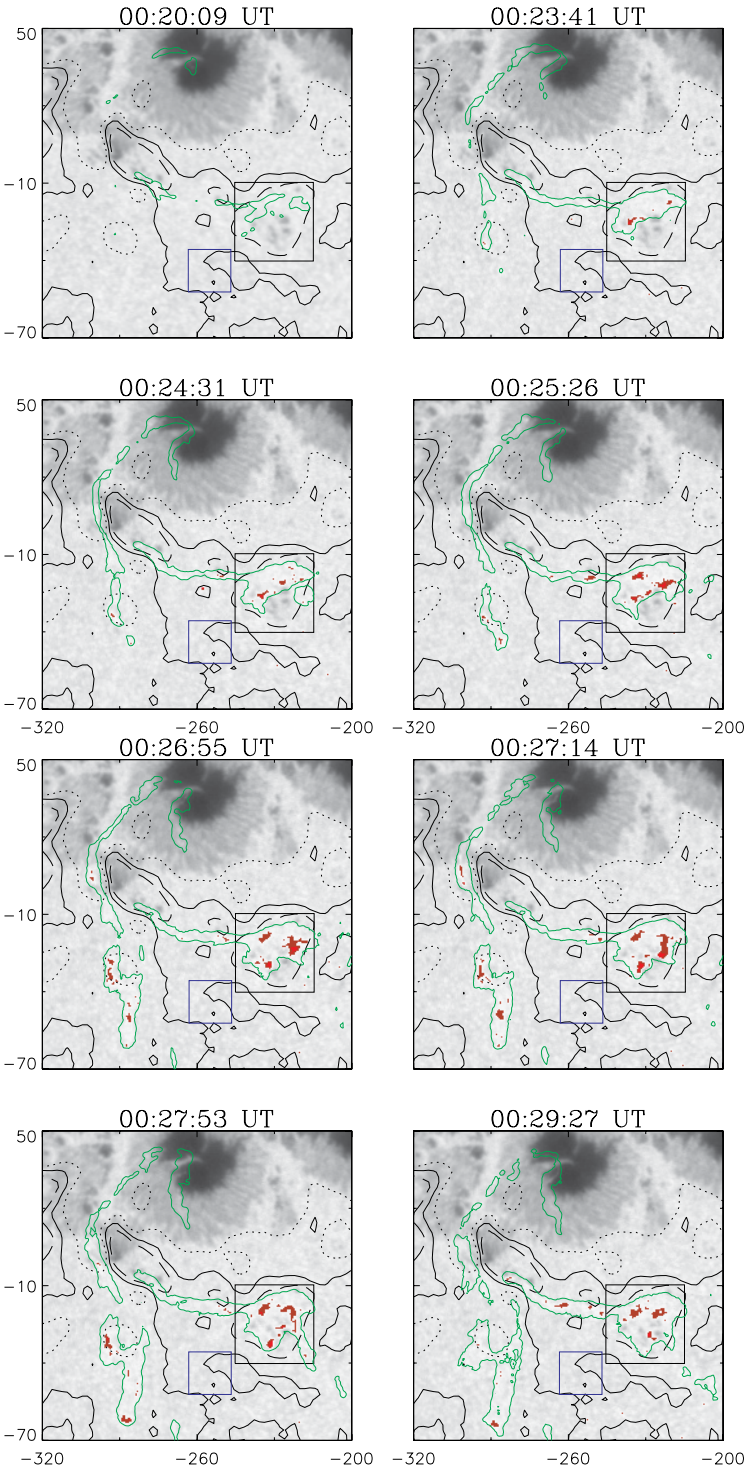

Fig. 1 TRACE WL images showing the evolution of the 2004 July 22 flare. The red patches are the identified strong enhancement in the WL images. The green lines are the contours of the 1700 Å enhancement, at level 10 times the mean count rate of the quiet-Sun; the thick black contours represent the magnetic neutral lines; the dotted/dashed contours indicate the positive/negative magnetic fields, at +100 and –100 Gauss, respectively. Note that the magnetogram is five-point smoothed in order to make the plot clear. The field of view is $2' \times 2'$.

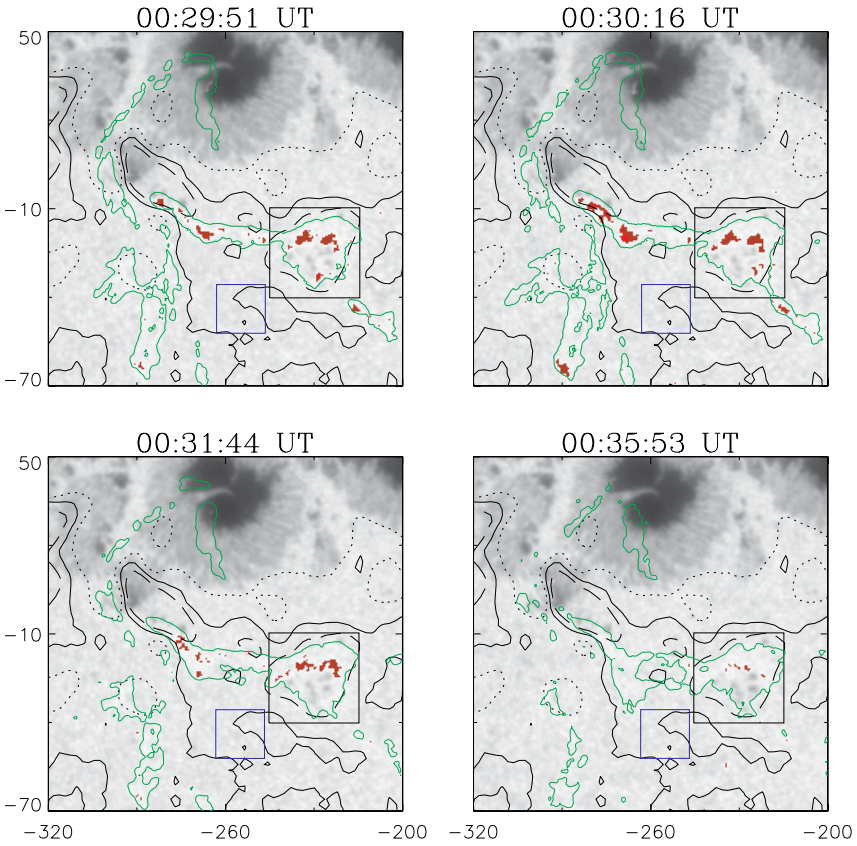

Fig. 1 *Continued.*

whose accuracy is 0.1 pixels. However, this method fails to correct the 1700 Å images, because the count rates of the small sunspots are a few tenths of the quiescent value. On the contrary, the count rate of some pixels reached several hundred times the quiescent value and varied dramatically during the flaring time. So we co-align each 1700 Å image with the previous one based on the near-quiescent part in the small region. This is done as follows.

We first select a reference image and co-align it with the following image by shifting the latter vertically or horizontally in steps of 0.125 pixels. Then we blink the shifted image and the reference image to see whether or not the part less affected by the flare is lined up in the two images. We repeat the above steps until all the nearly quiescent part of the two images is lined up. Then, the shifted image is taken as the reference image to correct the next image. The accuracy in lining up successive images is estimated to be 0.25 pixels or better. Considering that the alignment uncertainty of successive images may accumulate over the whole series of images, the final accuracy of alignment for all the 1700 Å images is estimated to be about 0.5 pixels. Finally, the corrected WL and 1700 Å images are co-aligned through a correlation check between the light curves extracted from the two data sets (see Sect. 3.3).

Figure 2 displays the jitter-effect-corrected WL images and the 1700 Å images closest in time, with the MDI magnetic field contours overlaid. Note that in order to highlight the enhancement, the contrast is defined as the ratio between a given count rate and the mean count rate from the statistical reduction.

It can be seen in Figure 2a that there are some small patches in the WL images with enhancements as high as 0.6 times the quiescent value. Correspondingly, in Figure 2b, there are similar small patches in the 1700 Å images with enhancements about 200 times the quiescent value. Actually, there are hundreds of such patches that appear at different times. They have a typical size of about $1'' - 2''$ and move along the

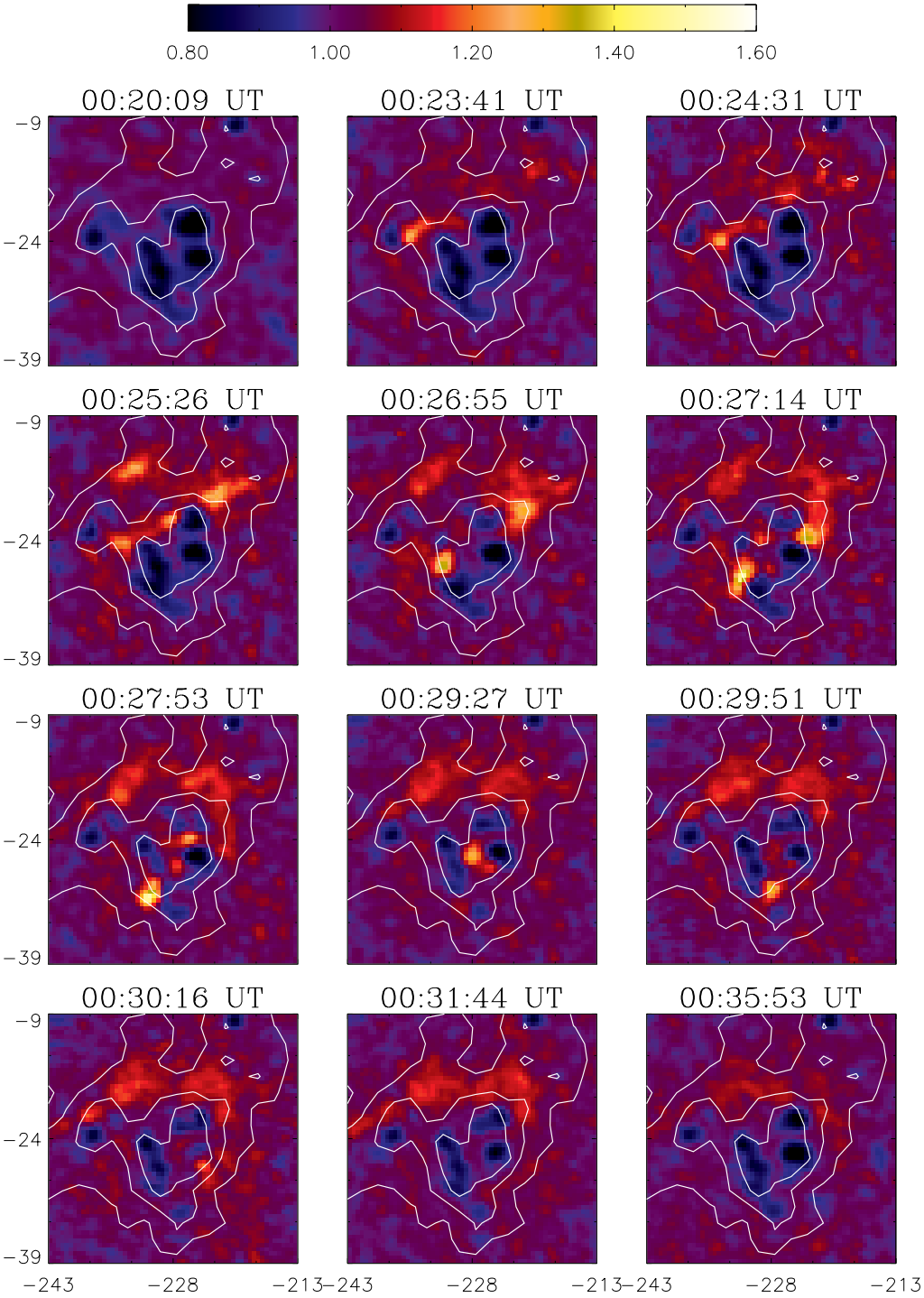

Fig. 2a TRACE WL images showing the evolution of the $30'' \times 30''$ small region indicated (the thick black box in Fig. 1). The contrast relative to the mean count rate of the quiet-Sun is shown by different colors. The solid lines show the MDI magnetic field contour levels of –500, –300, and –100 Gauss.

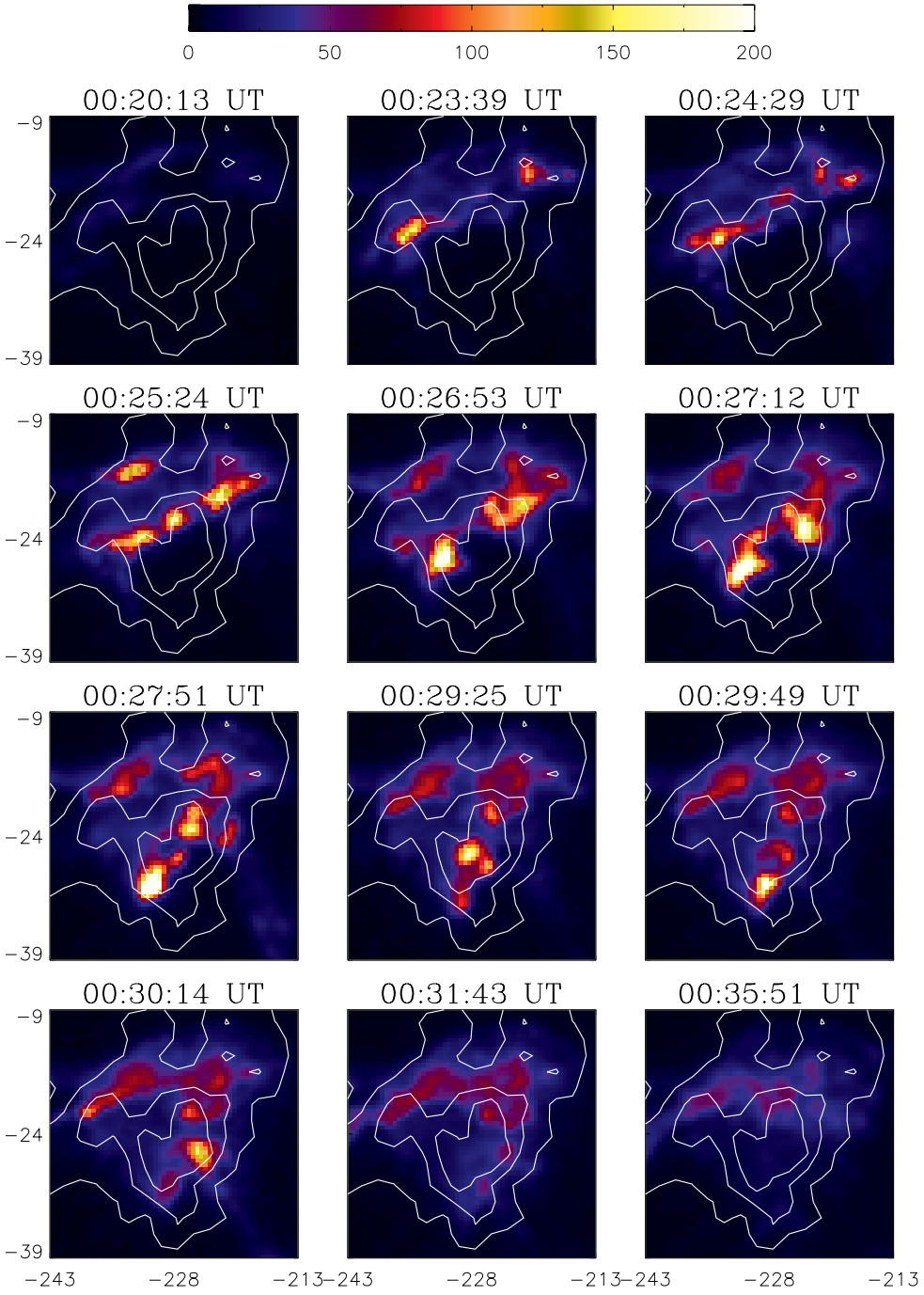

Fig. 2b Same as Fig. 2a but for the 1700 Å images.

magnetic field contour lines. Similar features have been reported previously (e.g., Fletcher & Warren 2003; Fletcher et al. 2004; Hudson et al. 2006).

We notice that the size mentioned above is close to the TRACE point-spread function, that is, about 3×3 pixels (Fletcher et al. 2004). Hence, the true size of the UV patches may be unresolved by TRACE observations, and the above size should be taken as an upper limit.

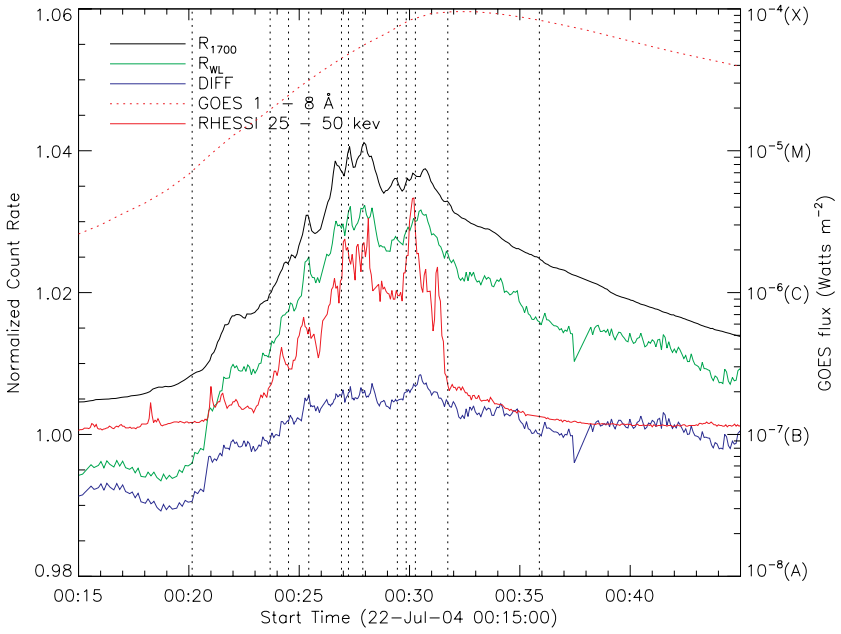

Fig. 3 TRACE light curves of the flare. $R_{\rm WL}$ is the ratio of the WL intensity to the mean value of the quiet-Sun (scale on left); R_{1700} the 1700 Å intensity in arbitrary units; DIFF refers to the difference between $R_{\rm WL}$ and 3.5 $\times$ R_{1700} (scale on left); GOES SXR flux is expressed in the units shown on the right; RHESSI 25–50 keV count rate of the whole Sun is plotted in arbitrary units. The vertical dotted lines mark the selected times in Figs. 1 and 2a.

Figure 3 displays the light curves averaged over this $30'' \times 30''$ area in the WL and 1700 Å channels. The RHESSI 25–50 keV HXR attenuator-corrected count rates and the GOES 1–8 Å SXR flux are also plotted for comparison. Obviously, the 1700 Å light curve is closely correlated to the WL light curve, as well as to the HXR count rates. The correlation coefficients between each pair of these three curves are determined. It is 0.986 between the 1700 Å and WL light curves, 0.793 between the 1700 Å and HXR, and 0.743 between the WL and HXR. The correlation between the 1700 Å and HXR emissions is rather more significant in the impulsive phase than in the decay phase, as can be seen clearly. This feature implies that the sharp enhancement of the 1700 Å emission is correlated with the non-thermal processes represented by the HXR emission.

The close correlation between the 1700 Å and WL light curves and the similarity between the images of the two bands are not reported previously (Metcalf et al. 2003; Hudson et al. 2006). It is important to clarify whether or not the small-scale enhancement comes from the UV band. Unfortunately, no UV spectrum was observed for the flare. Hence a precise comparison is unattainable. Metcalf et al. (2003) proposed that the UV portion in the WL images can be roughly removed by subtracting the weighted 1700 Å images. The authors gave a weighting factor of 7 for the quiet-Sun spectrum through a convolution calculation and pointed out that this factor may vary in different flare spectrum, reasonably over a range from 3.5 to 14. This method is taken as an alternative way to approximately estimate the contribution of the UV emission to the WL images. Considering the uncertainty of the UV spectrum under flare conditions, we use the lowest value, 3.5, for a conservative estimate. That is, we estimate a minimum UV contribution to the WL enhancement. The UV-corrected WL light curve is also plotted in Figure 3. It can be seen qualitatively that the WL enhancement is remarkably reduced. Though the subtraction is not a precise one, and the relationship between the white-light and UV continuum at the flaring time is still not very clear as of date, such a result supports to some extent that the WL brightenings in this region are mainly due to UV enhancement.

We emphasize that one must rule out the effect of the exposure-saturated pixels in the 1700 Å images to ensure the validity of the quantitative analysis. If some pixels in the flaring regions are exposure-saturated, then their intensity will be underestimated, and the above subtraction will give an overestimated result of WL emission that may degrade the validity of the conclusion. Fortunately, as mentioned in Section 2, the saturation effect in our observations is negligible and the images we used are valid for quantitative analysis.

Anyway, the small patches with sharp enhancement in 1700 Å images are attractive. A similar phenomenon has been reported in TRACE 1600 Å images as evidence of fine structures in the footpoints of coronal loops (e.g., Warren & Warshall 2001; Fletcher & Warren 2003; Fletcher et al. 2004). Below, we turn our attention to the 1700 Å images.

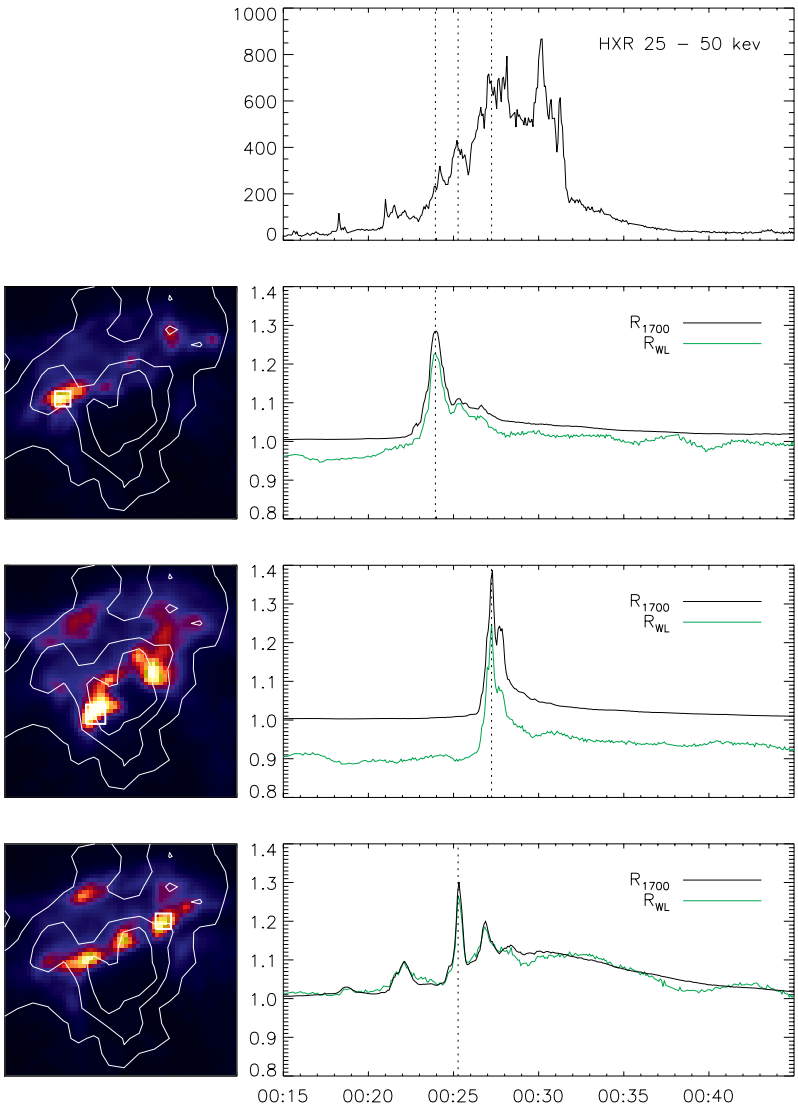

Fig. 4 Three examples of the light curves of small-scale brightenings. They are plotted with the same notation as in Fig. 3. The vertical dotted lines indicate the peak times of the enhancement. The HXR count rate is shown in the top panel. The TRACE 1700 Å images at the peak times are plotted to the left for reference in the same manner as Fig. 2b, with a white box in each of them which indicates the origin of the light curves.

3.3 Features of the Small-Scale UV Brightenings

To describe the features of the small-scale brightenings, we check their light curves. Here we show some examples. Figure 4 depicts three sets of light curves for three different small patches that appear at different times. In the three examples, the correlation coefficients between the WL and the corresponding 1700 Å light curves are all higher than 0.94. It confirms that the jitter-effect correction is working.

The three 1700 Å light curves all show a noticeable impulsive feature. The sharp increase and the quick decay in these light curves strongly imply that these small-scale brightenings may relate to non-thermal processes. Furthermore, the peaks of these 1700 Å light curves are around the sub-peaks of the HXR emission. This feature further confirms the non-thermal nature of these small patches that appear in the impulsive phase of the flare.

We quantitatively measure the enhancement of the UV emission in the 1700 Å images. The maximum enhancement in these three examples, averaged over the small white box, is about 150–200 times the mean count rate of the quiet-Sun. Note that the maximum count rate of individual pixels in the $30'' \times 30''$ region is found to be about 350 times the mean count rate of the quiet-Sun.

The full width at the half maximum (FWHM) of each enhancement is also evaluated. The measurement gives a typical timescale of about 30–60 s for these small-scale brightenings. We notice that the patches move rapidly around the fixed white boxes shown in Figure 4. The preceding and the following brightenings may contaminate the intensity in the boxes. This effect broadens the profiles of the impulsive feature in the 1700 Å light curves. Therefore, the timescale given in this work should be considered as an upper limit.

4 DISCUSSION

According to Handy et al. (1999), the emission involved in 1700 Å images is dominated by UV continuum. From the third panel of figure 9 in their work, the transmission of the combined 1600 Å and fused silica filters, which are used in the 1700 Å observations, gives a FWHM of about 170 Å (roughly from 1630 Å to 1800 Å). Though this wavelength range is included in that of the 1600 Å images, the emission of 1700 Å images is obviously different, because the latter includes a continuum with a narrower wavelength range and excludes the emission of strong lines, such as the C IV lines that come from the transition region. According to Brekke et al. (1996), the enhancement of the weak lines involved in the 1700 Å emission is comparable to the increase of the UV continuum. Hence, the contribution of the line emission to the broadband 1700 Å images is less than that of the continuum emission, and is therefore neglected below.

The continuum involved in 1700 Å images consists of the Si I photoionization continua with absorption limits at 1682 Å and 1985 Å. There have been some spectral observations on these continua. Cook & Brueckner (1979) found that there is lower enhancement in the UV radiation at longer wavelengths. The integrated 1420–1520 Å continuum in their two flares, which were both observed in the decay phase, is about 30–100 times brighter than the quiet-Sun continuum, and the integrated 1520–1680 Å continuum, 10–25 times brighter. No significant enhancement was observed at wavelengths longer than 1680 Å. Brekke et al. (1996) reported a similar result supporting this point of view in another flare, which was observed around the flare maximum. The UV continuum in their flare shows a higher enhancement at wavelengths shorter than 1550 Å, and a lower one at longer wavelengths. These spectral observations suggest that the 1700 Å enhancement comes mainly from the continuum emission at wavelengths shorter than 1680 Å (i.e., the continuum with absorption limit at 1682 Å).

The region of formation of the 1680 Å continuum is near the temperature minimum region (TMR), according to the model atmosphere calculations (e.g., Vernazza et al. 1976, 1981; Avrett et al. 1984). The temperature increase in the TMR during flares is due to the excessive absorption of radiation energy from both the chromosphere and the photosphere by enhanced H^- population (e.g., Ricchiazzi & Canfield 1983; Aboudarham & Hénoux 1986, 1987). Machado et al. (1986) indicated that the process of temperature rise in the TMR should be neither instantaneous nor impulsive. Hence, we infer that the gradual temperature increase in the TMR can not account for the impulsive UV enhancement presented in this work with 150–200 times the quiescent value, which corresponds to a brightness temperature increase of about 1600 K.

The theoretical calculations pointed out that the irradiation of C IV doublets (1548/1551 Å) in the transition region may play an important role in the 1680 Å continuum excitation under flare conditions (see Doyle & Phillips 1992 for review). Doyle & Phillips (1992) showed as well an observational near-proportional

relationship between the 1680 Å continuum intensity and the CIV 1548/1551 Å line intensity. Their conclusions lead to the interesting deduction that the 1700 Å enhancement during flares is indirectly due to the CIV emission, which is directly excluded from the 1700 Å images by the filters used in the observations.

Because there has been insufficient UV spectrum observations during flares so far and because of the difficulty of theoretical calculation under the flare conditions, we can only offer a possible interpretation of the emission mechanism for the 1700 Å enhancement on the basis of the above conclusions. That is, the impulsive increase of the 1700 Å emission might be due to an impulsive increase of the C IV1548/1551 Å line intensity. The latter might be caused by bombardment of the energetic electron beams that simultaneously produce the HXR emission. Therefore, the 1700 Å emission closely relates to the HXR emission, as revealed in our work. When the bombardment ends, the CIV line intensity, and hence the 1700 Å emission decreases rapidly. Previous works have pointed out that the locations of the UV brightenings are the footpoints of coronal loops, where the bombardment occurs. Hence our picture looks reasonable. However, before we reach a conclusion on the above process, more observational and theoretical investigations are needed.

Comparing the timescale of the HXR spikes or EFBs with that of the UV brightenings found in this work, we notice that the latter is significantly longer than the former. On the other hand, the timescale of UV brightenings is different from the flare duration. These facts imply that the brightenings correspond to an intermediate phenomenon between flares and EFBs or spikes. It reflects the reconnection process occurring in specific loops that are connected with the locations of the UV brightenings. Such a process may include a relatively stable reconnection and/or, many EFBs or spikes, which reflect the small-scale instability or turbulence in the reconnection process. Hence, the timescale found in this work may be important in the understanding of the physics of the reconnection. Furthermore, the study of these small-scale brightenings evidently builds a bridge for investigating the EFBs, when observations with higher cadence than that in this work become available.

5 SUMMARY

Using TRACE WL and 1700 Å data, we have analyzed the M9.1 two-ribbon flare that occurred on 2004 July 22. Our main results are summarized as follows:

1. We found many strongly enhanced small patches in TRACE WL images during the impulsive phase of the flare.
2. The enhancements in the WL and 1700 Å bands are highly correlated, and they are also closely correlated with the HXR emission.
3. The UV brightenings have a typical size of about 1″–2″ and a lifetime of about 30–60 s. The intensity enhancement is about 150–200 times the mean value of the quiet-Sun. We propose that these brightenings are related to non-thermal processes.

Acknowledgements We thank the referee for constructive comments that led to an improvement of the paper. We are grateful to all of the people who are responsible for the operations of the TRACE, RHESSI and SOHO/MDI instruments and who make the data available to use. This work was supported by the National Natural Science Foundation of China (NSFC) under grant Nos. 10221001, 10273023, 10333030, 10333040, 10403003, 10610099 and 10673004, as well as the grant from a 973 project 2006CB806302.

References

Abbett W. P., Hawley S. L., 1999, ApJ, 521, 906
Aboudarham J., Hénoux J. C., 1986, ApJ, 168, 301
Aboudarham J., Hénoux J. C., 1987, ApJ, 174, 270
Alexander D., Coyner A. J., 2006, ApJ, 640, 505
Aschwanden M. J., Hudson H., Kosugi T. et al., 1996, ApJ, 464, 985
Aschwanden M. J., Dennis B. R., Benz A. O., 1998, ApJ, 497, 972
Avrett E. H., Kurucz R. L., Loeser R., 1984, BAAS, 16, 450
Brekke P., Rottman G. J., Fontenla J. et al., 1996, ApJ, 468, 418
Canfield R. C., Gayley K. G., 1987, ApJ, 322, 999

Cheng C. C., Tandberg-Hanssen E., Bruner E. C. et al., 1981, ApJ, 248, L39
Cheng C. C., Tandberg-Hanssen E., Orwig L. E., 1984, ApJ, 278, 853
Cook J. W., Brueckner G. E., 1979, ApJ, 227, 645
Ding M. D., Qiu J., Wang H. et al., 2001, ApJ, 552, 340
Doyle J. G., Phillips K. J. H., 1992, A&A, 257, 773
Fletcher L., Warren H. P., 2003, in: K.-L. Klein ed., Energy Conversion and Particle Acceleration in the Solar Corona, Springer Lecture Notes in Physics, 612, 58
Fletcher L., Pollock J. A., Potts H. E., 2004, Sol. Phys., 222, 279
Fu Q. J., Yan Y. H., Liu Y. Y. et al., 2004, Chin. J. Astron. Astrophys. (ChJAA), 4, 176
Handy B. N. et al., 1999, Sol. Phys., 187, 229
Hudson H. S., Wolfson C. J., Metcalf T. R., 2006, Sol. Phys., 234, 79
Kanno M., Kurokawa H., the Hinotori Group, 1983, Sol. Phys., 86, 193
Kiplinger A. L., Dennis B. R., Emslie A. G. et al., 1983, ApJ, 265, L99
Kliem B., Karlický M., Benz A. O., 2000, A&A, 360, 715
Kurokawa H., Takakura T., Ohki K., 1988, PASJ, 40, 357
Lin R. P. et al., 2002, Sol. Phys., 210, 3
Machado M. E., Emslie A. G., Mauas P. J., 1986, A&A, 159, 33
Metcalf T. R., Alexander D., Hudson H. S. et al., 2003, ApJ, 595, 483
Nakajima H., 2000, in: R. Ramaty and N. Mandzhavidze ed., ASP Conf. Ser. 206, High Energy Solar Physics: Anticipating *HESSI*, San Francisco: ASP, p.313
Ricchiazzi P. J., Canfield R. C., 1983, ApJ, 272, 739
Scherrer P. H. et al., 1995, Sol. Phys., 162, 129
Trottet G., Rolli E., Magun A. et al., 2000, A&A, 356, 1067
Vernazza J. E., Avrett E. H., Loeser R., 1976, ApJS, 30, 1
Vernazza J. E., Avrett E. H., Loeser R., 1981, ApJS, 45, 635
Wang H., Qiu J., Denker C. et al., 2000, ApJ, 542, 1080
Warren H. P., Warshall A. D., 2001, ApJ, 560, L87
Zhao J. W., Fang C., Ding M. D., 1997, Sol. Phys., 173, 121